Reliability Engineering and Resilience 1-2 (2019) 46-66

Contents lists available at **RER**

Reliability Engineering and Resilience

Journal homepage: www.rengrj.com

Multi-Hazard Fragility Assessment of a Concrete Floodwall

S.S. Bodda[1*], A. Gupta[1], B. Ju[2], M. Kwon[3]

1. Center for Nuclear Energy Facilities and Structures, CCEE, North Carolina State University, Raleigh, USA
2. Institute for Disaster Prevention, Gangneung-Wonju National University, Gangneung, Republic of Korea
3. Department of Civil Engineering, Gyeongsang National University, Jinju, Republic of Korea
Corresponding author: *ssbodda@ncsu.edu*

https://doi.org/10.22115/RER.2020.214337.1017

ARTICLE INFO

Article history:
Received: 02 January 2020
Revised: 14 January 2020
Accepted: 29 January 2020

Keywords:
Seismic;
Flooding;
Probabilistic risk assessment;
Reliability;
Finite element.

ABSTRACT

Safety of critical industrial facilities such as Nuclear power plants has gained significant attention against external events in the last decade. Fukushima Daiichi nuclear power station disaster occurred due to flooding of the plant which was caused by the Great East Japan earthquake and the subsequent tsunami. In the US, failure of floodwall system during hurricane Katrina caused widespread damage. Floodwalls are essential to mitigate the effects of rising sea-levels due to climate change. Critical industrial facilities are being increasingly protected from the effects of floods through the use of flood protection systems such as floodwalls, dams, and weirs. This paper evaluates the fragilities for failure of a concrete floodwall due to various failure modes under a multi-hazard scenario (flooding and seismic events). Structural failure of the concrete floodwall is characterized by excessive deformation failure mode for seismic loads. The failure modes considered for flooding loads are rigid body failure and foundation failure.

1. Introduction

Fort Calhoun nuclear plant was shut down when the floodwall protecting vital areas at the plant collapsed during the historic Missouri river floods. Many industrial facilities are located near a body of water such as a river, a lake, an estuary or the sea because they require an abundant and

How to cite this article: Bodda S, Gupta A, Ju B, Kwon M. Multi-hazard fragility assessment of a concrete floodwall. Reliab. Eng. Resil. 2019;1(2):46–66. https://doi.org/10.22115/RER.2020.214337.1017.

dependable source of water. Floodwalls are also used to protect cities from the effects of rising sea levels due to climate change. In such and many other scenarios, the floodwall is required to safeguard against sustained reservoir levels. The seismic performance of a floodwall with sustained reservoir level can be very different from that of a floodwall with no water reservoir. Seismically induced failure of flood defense structures with sustained reservoir levels would result in flooding at critical facilities in the vicinity. These new and emerging conditions create a multi-hazard scenario which must be considered in the probabilistic risk assessment (PRA) for such external events. The two key components for calculating the risk of a flood defense structure are the fragility (probability of failure) and the hazard. In order to obtain the fragility of a flood defense structure, all critical failure modes must be accounted for and adequately expressed to represent the failure through the use of performance functions.

Various studies have been performed in the past to evaluate the fragilities for failure of flood defense structures under flooding and seismic events. Tekie and Ellingwood [1] present a methodology for developing seismic fragility and flooding fragility of concrete gravity dams. Lupoi [2] uses a similar approach to conduct the seismic fragility analysis of the Kasho dam. Ju and Jung [3] conduct seismic probabilistic risk assessment and its application to the case of the Gangjeong-Goryeong weir in Korea. Kaida and Miyagawa [4] describe a methodology for evaluating the fragility of a seawall against a tsunami. Rajabalinejad et al. [5] uses a probabilistic method integrated with finite element analysis to estimate the probability of failure of 17th street floodwall of New Orleans.

However, there are no existing studies on the probabilistic safety assessment (PSA) of a concrete floodwall considering a comprehensive set of failure modes particularly under a multi-hazard scenario. Furthermore, the effects of hydrodynamic pressure and seepage under the foundation have not been considered in the existing studies.

In this paper, we present the results from a study on evaluating the fragilities for failure of a concrete flood wall due to various failure modes under a multi-hazard scenario. The failure modes considered for flooding loads are rigid body failure and foundation failure. Rigid body failure is characterized by sliding and overturning of the floodwall. Failure of floodwall foundation is characterized by rupture and compression failure at the toe. For seismic loads, the structural failure of floodwall is characterized by excessive deformation. Finite element analysis is used for modeling the seismic behavior as well as the seepage through the foundation. Fragilities are evaluated by considering uncertainties in several variables that are used to characterize the earthquake input, reservoir levels, flood wall geometry, material properties, and local soil characteristics. A multi-hazard assessment of flooding and earthquake results in the evaluation of a fragility surface because both the flood hazard and seismic performance are correlated through the height of water in the reservoir. Such a fragility surface due to combined seismic and flooding events is evaluated in this paper.

2. Problem description

The failure of a floodwall during extreme flooding is typically a function of the height of reservoir pool. Higher water levels in the pool result in higher gradient for seepage through the

foundation and the consequent chances of a foundation failure are thereby increased. At the same time, the earthquake behavior of a floodwall is highly dependent upon the fluid-structure interaction between the water pool and the concrete structure. A higher level of reservoir results in greater hydrodynamic pressure leading to greater chances of failure. The study presented in this paper is carried out for a simple model of a floodwall.

3. Flooding fragility analysis

3.1. Failure in stability

A floodwall can fail by rigid body failure mechanism (either due to overturning or sliding) or crushing failure of the foundation or concrete. Fig. 1 shows the loads that are normally considered for the stability analysis of a floodwall and are described below.

3.1.1. Loads acting on the floodwall

Gravity Load: The gravity load acting downward is taken to be the total weight of the flood wall, retaining water above the heel, and weight of the soil over the heel and the toe. The weight of the section per unit length is equal to the area of the cross-section times the specific weight of the material. The load acts vertically downwards through the center of gravity of the sections as shown in Fig. 1.

weight of the wall (N/m)	:	$w_w = H_w t_w \gamma_c$	(1)
weight of the footing (N/m)	:	$w_f = B t_f \gamma_c$	(2)
weight of the retaining water above the heel (N/m)	:	$w_{rw} = (H + D_h) B_h \gamma_w$	(3)
weight of the soil over the heel (N/m)	:	$w_{sh} = D_h B_h (\gamma_s - \gamma_w)$	(4)
weight of the soil over the toe (N/m)	:	$w_{st} = D_t B_t \gamma_s$	(5)

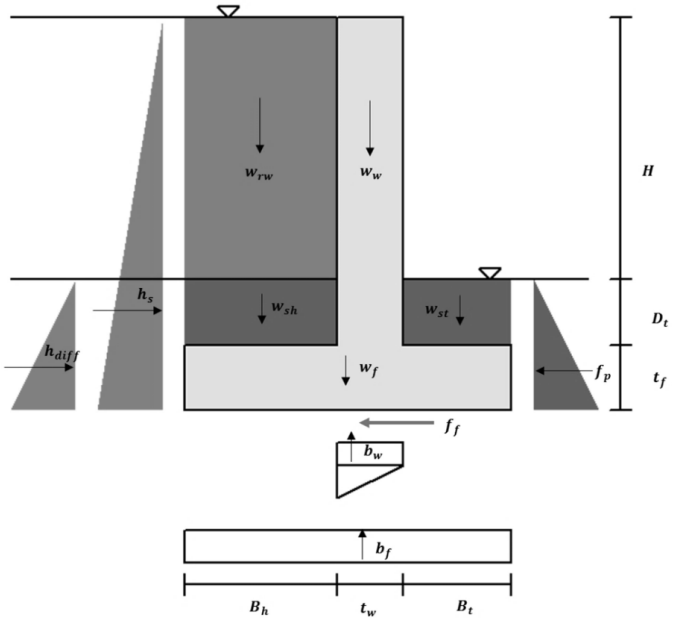

Fig. 1. Loads acting on the floodwall.

B = footing width
H_w = wall height
H = upstream water level
t_w = wall thickness
t_f = footing thickness
D_t = depth of the soil above the toe
D_h = depth of the soil above the heel
B_t = toe width
B_h = heel width
γ_c = specific weight of concrete
γ_w = specific weight of water
γ_s = specific weight of soil
k_p = passive soil pressure coefficient
G_s = specific gravity of soil
H_{ds} = downstream water level
S = equivalent fluid weight of submerged soil and water

Hydrostatic Forces: Water that lies below or above the ground surface causes hydrostatic loads. Various types of loads that contribute to the hydrostatic loads are lateral hydrostatic loads, uplift loads at the bottom of foundation, and differential saturated soil force acting in the horizontal direction beneath the ground surface. Hydrostatic pressures increase linearly with the depth of water above or below the point under consideration and are equal in all directions.

lateral hydrostatic force (N/m) : $$h_s = 0.5\gamma_w\left(H + D_h + t_f\right)^2 \quad (6)$$

differential saturated soil/water force (N/m) : $$h_{diff} = 0.5(S - \gamma_w)\left(D_h + t_f\right)^2 \quad (7)$$

buoyancy force on the footing (N/m) : $$b_f = \gamma_w B t_f \quad (8)$$

buoyancy force on the wall (N/m) : $$b_w = 0.5\gamma_w t_w (H + D_t + D_h) \quad (9)$$

Frictional Force: The sliding frictional force, f_f acting along the base of the foundation is proportional to the net vertical force f_v and the coefficient of friction μ_f.

frictional force (N/m) : $$\begin{aligned} f_f &= f_v \mu_f \\ f_v &= \left(w_w + w_f + w_{rw} + w_{sh} + w_{st}\right) - \left(b_w + b_f\right) \end{aligned} \quad (10)$$

Lateral Passive Earth Force: The passive earth pressure is generated when the soil mass is compressed outward due to the floodwall pushing on it.

passive saturated soil force (N/m) : $$f_p = 0.5\left[k_p(\gamma_s - \gamma_w) + \gamma_w\right]\left(D_t + t_f\right)^2 \quad (11)$$

3.1.2. Performance functions

In this study, three performance functions are used to characterize the stability failure and evaluate the corresponding fragilities. These three performance functions are described below.

Sliding Failure: Sliding failure occurs if the horizontal forces due to lateral hydrostatic loads exceed the floodwall resistance due to frictional and passive soil loads, thereby causing the floodwall to slide horizontally as an entire unit as shown in Fig. 2. The performance function for sliding failure is characterized by the following limit state:

$$Z_s = \sum R_H - \sum F_H \tag{12}$$

$$\sum R_H = f_p + f_f \qquad \sum F_H = h_s + h_{diff} \tag{13}$$

where: $\sum R_H$ is the total resistive force, $\sum F_H$ is the total horizontal force

The probability of failure due to sliding of the flood wall is given by:

$$P_f(sliding) = P(Z_s < 0) \tag{14}$$

Overturning of the flood wall: Wall overturning occurs if the overturning moments due to the hydrostatic forces exceeds the floodwall resistive moments due to all vertical downward forces and passive soil load about the toe, thereby causing the floodwall to topple or rotate as shown in Fig. 2. The performance function for overturning failure is characterized by the following limit state:

$$Z_o = \sum M_R - \sum M_O \tag{15}$$

where: $\sum M_R$ is the total resisting moment about the toe, and $\sum M_O$ is the overturning moment

$$\sum M_R = w_w(A_t + 0.5t_w) + w_f(0.5B) + w_{sh}(B - 0.5A_h) + w_{st}(0.5A_t) + w_{rw}(B - 0.5A_h) + f_p\left(\frac{D_t + t_f}{3}\right) \tag{16}$$

$$\sum M_O = h_s\left(\frac{H + D_h + t_f}{3}\right) + h_{diff}\left(\frac{D_h + t_f}{3}\right) + b_f(0.5B) + b_{w1}(A_t + 0.5t_w) + b_{w2}\left(\frac{2}{3}t_w + A_t\right) \tag{17}$$

The probability of failure due to overturning of the floodwall is given by:

$$P_f(overturning) = P(Z_o < 0) \tag{18}$$

Compression failure of foundation at the toe of the floodwall: Compression failure of the foundation at the toe occurs if the pressure on the foundation, p_n exceeds the allowable soil bearing capacity, σ_b^f. The performance function for compression failure of foundation at the toe is characterized by the following limit state:

$$Z_{cf} = \sigma_b^f - p_n \tag{19}$$

$$p_n = \frac{f_v}{B}\left(1 + \frac{6e}{B}\right) \tag{20}$$

where, distance e is the eccentricity from the centerline of the footing and represents the location of resultant force.

$$e = \frac{B}{2} - \frac{M_R - M_O}{f_v} \tag{21}$$

The probability of failure of foundation due to compression at toe is given by:

$$P_f(compression\_toe) = P\left(Z_{cf} < 0\right) \tag{22}$$

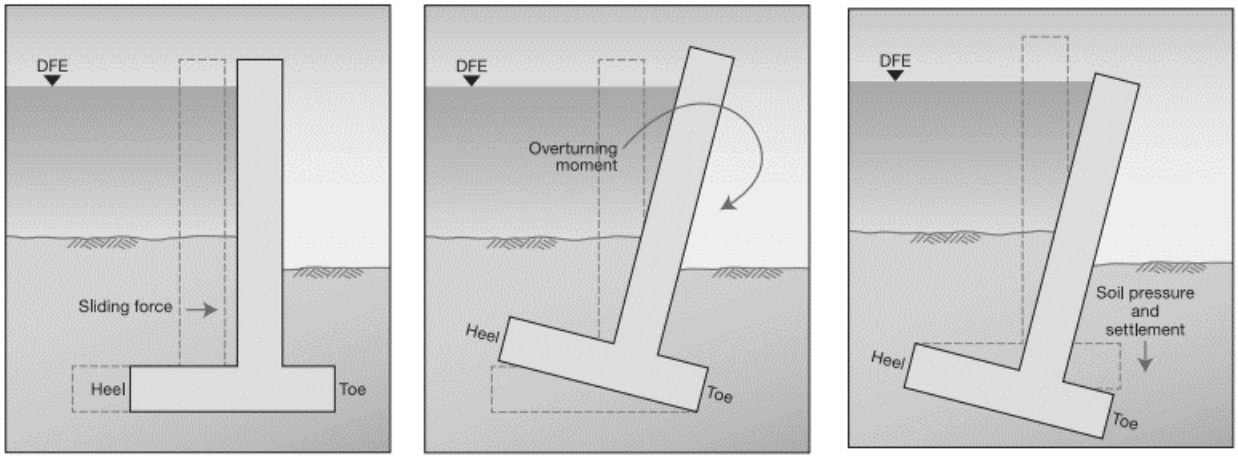

Fig. 2. Failure by sliding, overturning, and compression failure of foundation (FEMA259 [6]).

3.1.3. Fragility curves for stability failure

Fragility curves are one of the key components of probabilistic risk assessment. The fragility curve gives the conditional probability of failure over the complete range of loads to which that system might be exposed in its lifetime. The uncertainties in the random variables that characterize the performance function are incorporated using Monte Carlo simulations. The parameters to be taken as random variables are chosen in accordance with the existing studies ([6,7]) and are shown in Table 1. The analysis is carried out for 100,000 random samples with different heights of upstream water level ranging from 0 to 5 meters to calculate the probability of failure. Fragility curves due to sliding failure are shown in Fig. 3 and fragility curves due to compression failure of foundation at toe are shown in Fig. 4. The fragility curves are generated for two classes of soils, Class-2 and Class-3 according to the Table 3285.202 of ASTM D 2487-00 [8]. The soil foundation at the site consists of silty sand which belongs to Class-3.

The fragility curve due to sliding failure for Class-3 soil shows greater uncertainty than the Class-2 soil due to a larger uncertainty in the coefficient of friction for Class-3 soil. The fragility curves are not plotted for overturning failure mode as the total resistive moments are greater than the overturning moments. The fragility curves for compression failure of foundation at the toe are governed by the allowable soil bearing capacity.

Table 1
Random variables and deterministic values used to evaluate Fragility curves.

Variable	**Distribution**	**Parameters/moments**
H_{ds} (m)	Deterministic	0
g (m/s^2)	Deterministic	9.81
S (kN/m^3)	Normal	$Soil\ Class-2: \mu_S = 12, \sigma_{C_f} = 0.12$ $Soil\ Class-3: \mu_{C_f} = 13, \sigma_{C_f} = 0.195$
γ_w (kN/m^3)	Deterministic	9.804
γ_c (kN/m^3)	Normal	$\mu_{\gamma_c} = 25, \quad \sigma_{\gamma_c} = 1$
G_s (-)	Normal	$\mu_{G_s} = 2.66, \quad \sigma_{G_s} = 0.01$
μ_f (-)	Normal	Soil Class $-$ 2 : Uniform[0.55 0.60] Soil Class $-$ 3 : Uniform[0.35 0.55] Silty Sand : Uniform[0.45 0.55]
k_p (-)	Normal	$\mu_{k_p} = 3.5, \quad \sigma_{k_p} = 0.3$
σ_b^f (kN/m^2)	Normal	$Soil\ Class-2: \mu_{k_p} = 95, \sigma_{k_p} = 2$ $Soil\ Class-3: \mu_{k_p} = 70, \sigma_{k_p} = 2$
$D_t = D_h$ (m)	Deterministic	0

where: μ is the mean, σ is the standard deviation

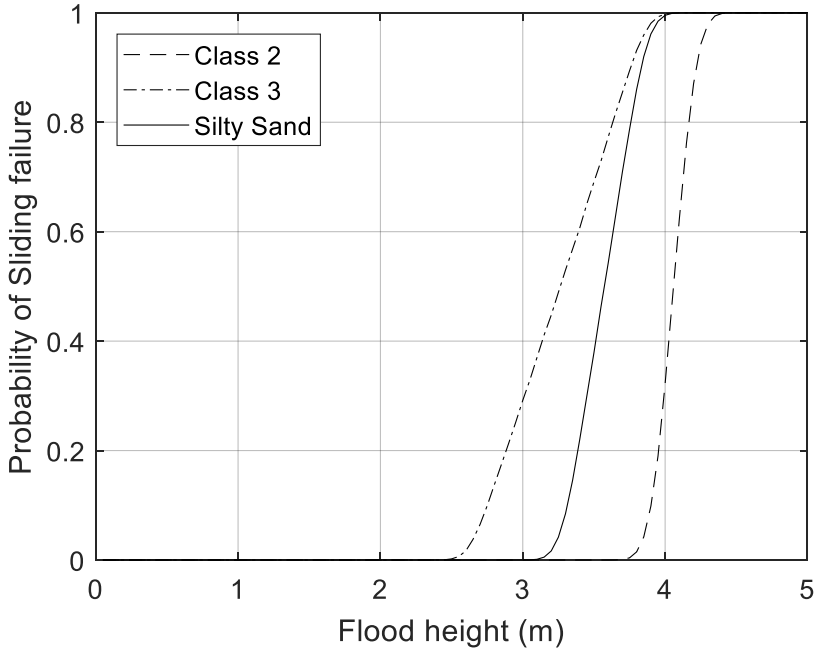

Fig. 3. Fragility curve due to Sliding Failure**.**

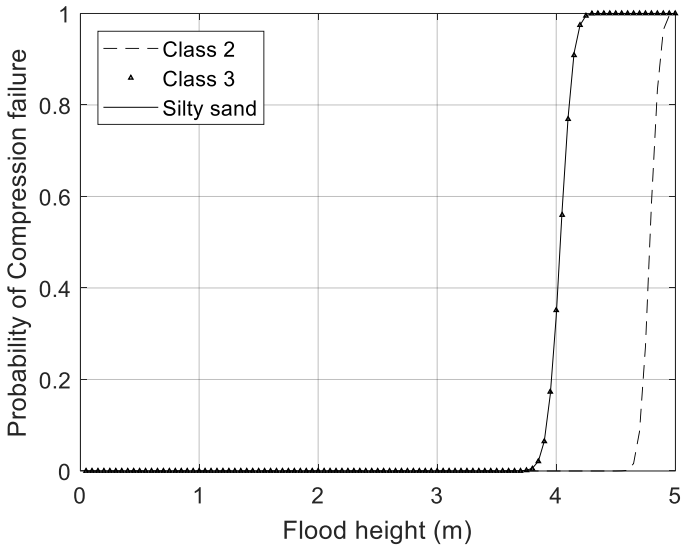

Fig. 4. Fragility curve due to Compression Failure of Foundation at the Toe.

3.2. Failure in instability

Seepage analysis plays an important role in the design of flood defense structures. Uncontrolled seepage can cause excessive uplift pressures and internal erosion of the material at the downstream leading to a piping phenomenon through the embankment and the foundation. A piping phenomenon is initiated when the rupture of the foundation occurs, and the rupture takes place if the critical hydraulic gradient (i_{cr}) is lesser in magnitude than the maximum exit gradient (i_{ex}). For the accurate calculation of seepage gradients under the flood defense structures, numerical methods are usually adopted. In this study, finite element method is used for solving the seepage problem as it can capture the effects of complex boundaries and soil anisotropy accurately.

Based on Darcy's law, the discharge velocity for a homogeneous, anisotropic soil is given by:

$$v_n = -k_n \frac{\partial h}{\partial n} \quad (23)$$

$$v_n = -k_n \frac{\partial h}{\partial n} \ \#(1)$$

where: v is the discharge velocity or seepage flow, h is the total hydraulic head, and k is the hydraulic conductivity.

The differential equation governing the steady-state flow is expressed as:

$$k_x \frac{\partial^2 h}{\partial x^2} + k_y \frac{\partial^2 h}{\partial y^2} = 0 \quad (24)$$

For the critical hydraulic gradient, the following expression by Terzaghi [9] is used:

$$i_{cr} = \frac{G-1}{1+e} = (G-1)(1-n) \quad (25)$$

where: G is the specific gravity of the soil, n and e are the porosity and void ratio of the soil.

The governing equations and boundary conditions to be applied in order to solve the two-dimensional partial differential equation of the seepage problem are shown in Fig. 5 and discussed below:

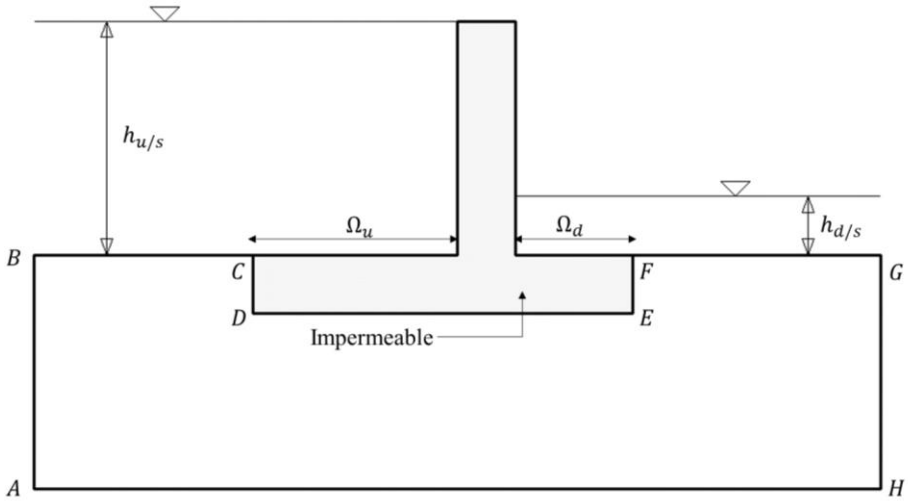

Fig. 5. Boundary conditions for the seepage analysis.

Hydraulic head boundary conditions: Hydraulic head on the upstream side (BC and Ω_u) of the floodwall is equal to the upstream water level, $h_{u/s}$. Hydraulic head on the downstream side (FG and Ω_d) of the floodwall is equal to the downstream water level, $h_{d/s}$.

$h = h_{u/s}$ on BC and Ω_u, $\quad h = h_{d/s}$ on FG and Ω_d

Seepage flow boundary conditions: No flow boundary conditions are imposed on the impermeable concrete floodwall (CD, DE, EF) and the elastic half space (AB, GH, AH).

$k_n \frac{\partial h}{\partial n} = 0$ on AB, CD, DE, EF, GH, AH.

Fragility Curve for Rupture failure

The finite element model for the seepage analysis is developed by following the concepts described in Bodda and Gupta [10]. Based on the convergence study, the dimensions of the elastic half space are found out to be upstream width, $B_1 = 15\,m$; downstream width, $B_2 = 15\,m$; depth, $D = 20\,m$.

In this study for calculating the probability of rupture failure, uncertainties in both the capacity and the demand are considered. The capacity, critical gradient is a function of specific gravity and porosity of the soil. The demand, maximum exit gradient is a function of anisotropic ratio (k_y/k_x) and upstream flood water level.

The limit state equation or performance function is expressed as the difference between capacity, i_{cr}, and demand, i_{ex}:

$$Z_R = i_{cr} - i_{ex} \tag{26}$$

The conditional probability of rupture failure given upstream flood water level (H) is expressed as:

$$P_f(rupture|H) = P(Z_R < 0) \tag{27}$$

The fragility curve is generated using Monte Carlo simulations by considering all the uncertainties in both the capacity and the demand (Table 2). A set of 200 random samples are generated from each of the random variables. The fragility analysis is carried out for such 200 samples per each upstream water level ranging from 0 to 5 m. The fragility curve due to rupture failure is shown in Fig. 6.

Table 2
Random variables and deterministic values used to evaluate Fragility curves

Variable	Distribution	Parameters/moments
k_y/k_x (-)	Normal	$\mu_K = 0.5$ $\sigma_K = 0.18$
n (-)	Normal	$\mu_n = 0.46$ $\sigma_n = 0.05$
G_s (-)	Normal	$\mu_G = 2.66$ $\sigma_G = 0.01$

where: μ is the mean, σ is the standard deviation, H_{ds} – Height of downstream water level

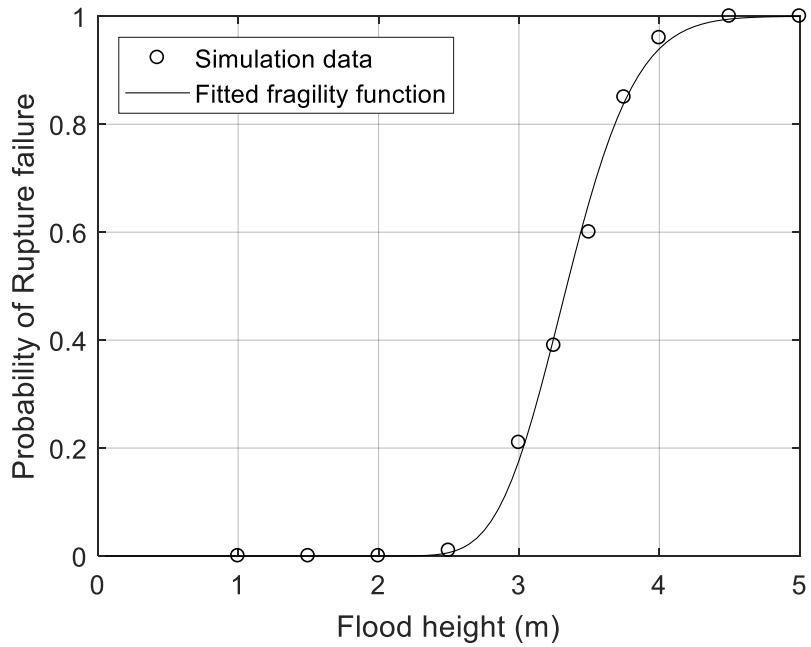

Fig. 6. Fragility curve due to Rupture Failure.

3.3. System level flooding fragility

The system level flooding fragility is evaluated by considering the effect of all the failure modes of a floodwall. Considering all these modes as independent, the combined fragility of failure due to a flooding hazard is calculated using the following expression:

$$P(system|flood\ height) = \cup_i P(LS_i|flood\ height) \quad (28)$$

where, $P(LS_i|flood\ height)$ is the fragility of i^{th} failure mode.

The system level flooding fragility curve is shown in Fig. 7. The failure probability for system level at different flood heights is governed by different failure modes. Rupture failure mode governs until a flood height of 3.3 m and sliding failure mode governs after a flood height of 4 m. In this analysis, the effect of compression failure mode is negligible as compared with other failure modes.

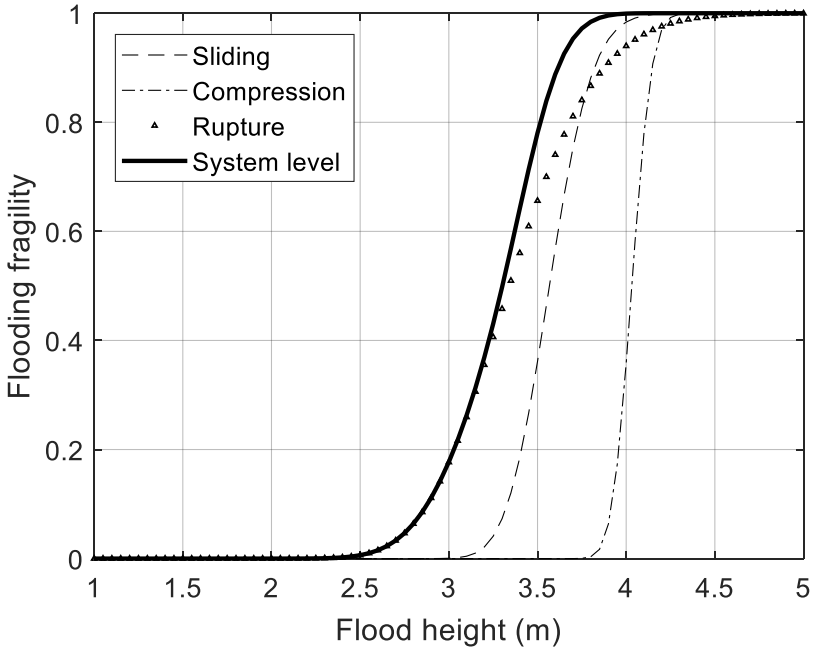

Fig. 7. System level Flooding Fragility curve.

4. Seismic fragility analysis

In this section, the effect of various ground motions on the seismic response of floodwalls is investigated. Finite element analysis is used for modeling the seismic behavior of the floodwall. The modeling concepts described in detail in Bodda et al. [11] for the analysis of a concrete gravity dam are used for modeling the floodwall. The formulations and associated concepts are discussed below.

4.1. Fluid structure interaction (FSI) formulation

A large number of existing studies assume that the fluid is incompressible in a fluid-structure interaction analysis. However, Akhaveiss and Malekshahi [12] illustrate that the consideration of fluid compressibility in such analyses results in higher hydrodynamic pressures on the upstream face of the structure. Therefore, the fluid is modeled as compressible in the study described below.

The two-dimensional wave equation for a fluid is obtained from the combined Navier-Stokes equations of fluid momentum and the flow continuity equation by assuming that the fluid is compressible. Compressibility is defined as changes in fluid density due to pressure variations. The viscosity is neglected, and the mean density and pressure are considered to be uniform throughout the fluid:

$$\frac{1}{c^2}\frac{\partial^2 P}{\partial t^2} - \nabla^2 P = 0 \tag{29}$$

where, $P = P(x, y, t)$ is the acoustic pressure, c is the acoustic wave speed, and t is the time. If the fluid is incompressible then Eq. (29) simplifies to:

$$\nabla^2 P = 0 \tag{30}$$

Eq. (23) is used to solve the fluid-structure interaction problem by imposing the following boundary conditions [13] on the fluid domain as shown in Fig. 8.

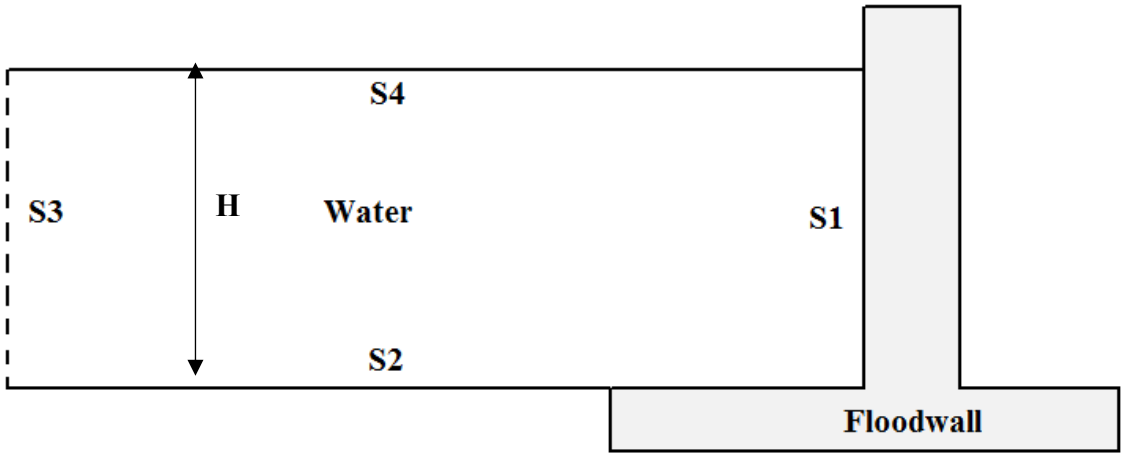

Fig. 8. Boundary conditions of the Fluid domain.

Fluid Boundary Conditions

Fluid-Structure Interface (S1) – At this boundary, the pressure gradient is equal to the inertial force caused by the movement of reservoir wall. Therefore,

$$\frac{\partial P}{\partial n} = -\rho \ddot{U}_n \tag{31}$$

where *n* is the unit vector normal to the interface, $\ddot{U}_n$ is the normal acceleration of structure at the interface.

Reservoir bottom (S2) – It is assumed that the incident hydrodynamic pressure waves gets absorbed by the material at the bottom of reservoir bottom. To account for this assumption at boundary S2, a damping coefficient $\bar{q}$ is incorporated.

$$\frac{\partial P}{\partial n} = -\rho \ddot{U}_n - \bar{q}\frac{\partial P}{\partial t}, \ \alpha = \frac{1-\bar{q}c}{1+\bar{q}c} \tag{32}$$

where α is the wave reflection coefficient, defined as the ratio of the amplitude of the reflected pressure wave to that of the normally incident wave. The value of α is typically selected based on the properties of material that forms the reservoir bed. A value of α equal to zero represents a soft reservoir bed such that all the waves are absorbed and a value of 1 represents a rigid foundation such that all the waves are reflected back [14].

Reservoir upstream boundary (S3) – At this boundary, the outgoing hydrodynamics waves generated due to the vibration of wall should continue to propagate outward but not inward. This condition is termed as sommerfeld radiation boundary condition [15].

$$\frac{\partial P}{\partial n} = -\frac{1}{c}\frac{\partial P}{\partial t} \tag{33}$$

Reservoir free surface (S4) – At the free surface, surface waves are neglected which can be represented as:

$$P(x, y = H, t) = 0 \tag{34}$$

Finite Element Formulation

The finite element shape functions for the spatial variation of the fluid pressure P and the structural displacement u are given by:

$$P = \{N\}^T\{P_e\},\ u = \{N'\}^T\{U_e\} \tag{35}$$

where

$\{P_e\}$ = nodal pressure vector
$\{U_e\}$ = nodal structural displacement vector
$\{N\}$ = element shape function for pressure
$\{N'\}$ = element shape function for displacement

Discretized Fluid Equation

The discretized wave equation at the fluid structure interface is given by:

$$[M_e^P]\{\ddot{P}_e\} + [C_e^P]\{\dot{P}_e\} + [K_e^P]\{P_e\} + \rho_w[R_e]^T\{\ddot{U}_e\} + \rho_w[R_e]^T[I]\ddot{u}_g = \{0\} \tag{36}$$

where

$$[M_e^P] = \frac{1}{c^2}\int \{N\}^T\{N\}d\Omega \quad \text{fluid mass matrix}$$

$$[K_e^P] = \int \{\nabla N\}^T\{\nabla N\}d\Omega \quad \text{fluid stiffness matrix}$$

$$[C_e^P] = \frac{1}{c}\int \{N\}^T\{N\}d\Gamma \quad \text{fluid damping matrix}$$

$$\rho_w[R_e] = \rho_w\int \{n\}^T\{N\}\{N'\}^T d\Omega \quad \text{coupling mass matrix}$$

Discretized Structure Equation

The equation of motion for the structure at the element level is given by:

$$[M_e]\{\ddot{U}_e\} + [C_e]\{\dot{U}_e\} + [K_e]\{U_e\} = -[M_e]\{\Gamma\}\ddot{u}_g + [R_e]\{P_e\} \tag{37}$$

where $\{\Gamma\}$ is an influence vector which transmits the support acceleration $\ddot{u}_g$ to structural degrees of freedom and $[R_e]\{P_e\}$ represents the nodal force vector associated with the hydrodynamic pressure caused by the fluid.

Discretized Fluid-Structure Coupling Equation

The complete finite element discretized equations for the fluid-structure interaction problem are expressed as:

$$\begin{bmatrix} [M_e] & [0] \\ [M^{fs}] & [M_e^P] \end{bmatrix} \begin{Bmatrix} \{\ddot{U}_e\} \\ \{\ddot{P}_e\} \end{Bmatrix} + \begin{bmatrix} [C_e] & [0] \\ [0] & [C_e^P] \end{bmatrix} \begin{Bmatrix} \{\dot{U}_e\} \\ \{\dot{P}_e\} \end{Bmatrix} + \begin{bmatrix} [K_e] & [K^{fs}] \\ [0] & [K_e^P] \end{bmatrix} \begin{Bmatrix} \{U_e\} \\ \{P_e\} \end{Bmatrix} = \begin{Bmatrix} -[M_e]\{\Gamma\}\ddot{u}_g \\ -\rho_w[R_e]^T\{\Gamma\}\ddot{u}_g \end{Bmatrix} \tag{38}$$

where

$$[M^{fs}] = \rho_w[R_e]^T \text{ and } [K^{fs}] = -[R_e] \tag{39}$$

Coupling Matrix $[R_e]$ transforms both the structure acceleration and the support acceleration to pressure flux and also transforms the hydrodynamic pressure into applied loads to the structure (ANSYS [16]).

4.2. Modeling of floodwall and reservoir system

In this study, two-dimensional 4-noded structural solid and 4-noded acoustic fluid elements are used to discretize the solid floodwall and the reservoir water, respectively [16]. The floodwall is assumed to be linearly elastic and in a state of plane stress. The reservoir is assumed to be of uniform shape and water is considered to be a compressible and inviscid fluid. The foundation of the floodwall reservoir system is assumed to be rigid. The length of the reservoir is chosen as two times the floodwall height [17] and the surface waves are neglected. Impedance loading condition which relates to the incident and reflected waves at the S3 boundary is used for absorbing the waves.

The two-dimensional finite element model of the floodwall reservoir system is shown in Fig. 9. The concrete is assumed to be homogeneous and isotropic with elasticity modulus of 22400 MPa, poison's ratio of 0.20, and density of 2480 kg m^{-3}. The density and the velocity of the pressure wave in water are taken as 1000 kg m^{-3} and 1440 m/s respectively.

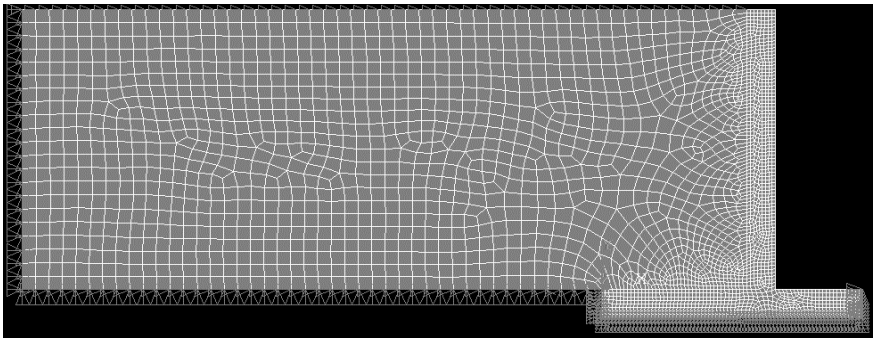

Fig. 9. Finite element model of Floodwall Reservoir system.

4.3. Time history analysis of reservoir-floodwall system

The linear transient dynamic analysis for the concrete floodwall is performed using direct integration method. In this model, Rayleigh damping is used for the dynamic analysis. Therefore, modal analysis of the FE model is carried out to calculate the Rayleigh damping coefficients. In this study for the modal analysis, damped mode-extraction method is used. This method is employed as it accounts for the damping due to impedance boundary condition at S3 and unsymmetrical mass and stiffness matrices due to the fluid structure interaction. Complex eigenvalues are obtained from the damped modal analysis. The real part of the eigenvalue physically represents the stability of the system and the imaginary part of the eigenvalue represents the natural frequency of the system. The first three natural frequencies of the reservoir-floodwall system are 6.37 Hz., 36.87 Hz., and 85.54 Hz. Clearly, the response of the floodwall for the seismic motion is primarily from the first two modes. Therefore, damping ratio of 5% are chosen for the first and the second vibration modes.

A time step of 0.005 seconds is chosen for the unconditionally stable implicit time marching scheme. The response of the floodwall is evaluated for 1975 Oroville earthquake scaled to 0.1g PGA (Fig. 10) and the time history of horizontal displacement at the wall crest is plotted as shown in Fig. 11. The maximum displacement (Δ_D) obtained from the displacement time history at the wall crest is used for calculating fragility due to the excessive deformation failure mode. The hydrodynamic pressure envelope acting on the upstream face of the floodwall is shown in Fig. 12. This pressure envelope is very similar to what is observed in prior studies for concrete dams [18].

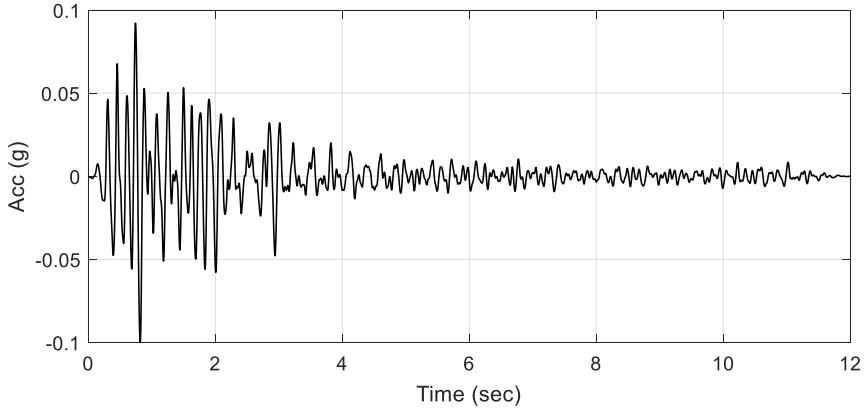

Fig. 10. Acceleration Time History of Oroville earthquake scaled to 0.1g PGA.

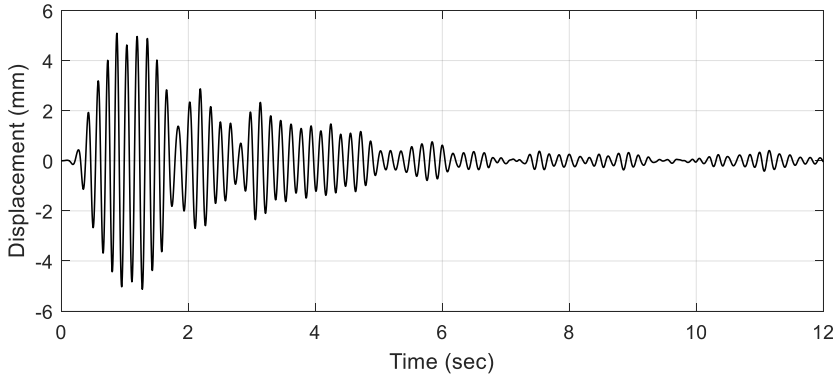

Fig. 11. Horizontal displacement time history at the wall crest with full reservoir**.**

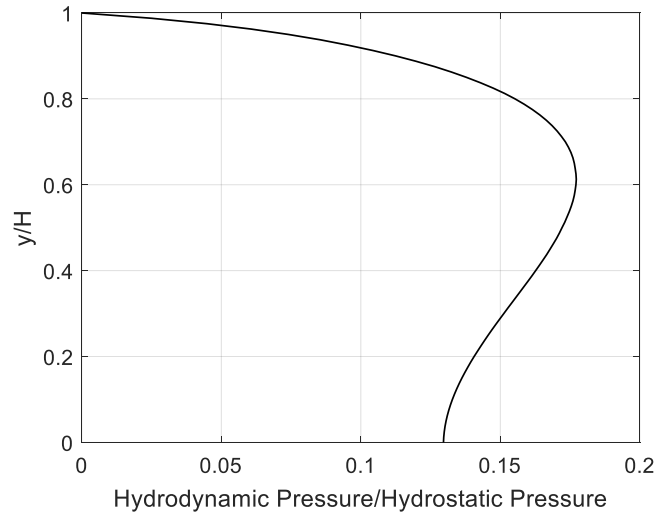

Fig. 12. Hydrodynamic Pressure envelope acting on the upstream face of the Floodwall.

4.4. Seismic fragility surface

Seismic fragility curves for the floodwall are evaluated by considering 10 recorded time histories as shown in Table 3. The response spectra of the ten ground motions scaled to 1g are shown in Fig. 13 for a damping ratio of 5%. Many of these spectra have peaks in the range of 6-7 Hz. and the first mode of the floodwall is 6.37 Hz. But some of these spectra also have peaks in the high frequency region and it can excite the second mode of the floodwall. Therefore, this fragility analysis can capture the effect of both low and high frequency modes.

Each ground motion is scaled to yield PGA values ranging from 0.1g to 0.8 g as an input for the floodwall model. A total of 10 finite element simulations are carried out for each PGA with a reservoir level of 2.5 m. The fragility analysis is carried out for material properties described in section 4.2 and the uncertainty is considered only in the seismic ground motions. Structural performance is evaluated with respect to the excessive deformation failure mode given by:

$$Z_{\Delta} = \Delta_C - \Delta_D \tag{40}$$

where, Δ_D = maximum crest displacement and Δ_C = 0.05% of height of the floodwall [1]

The conditional probability of excessive deformation failure given peak ground acceleration (PGA) is expressed as:

$$P_f(excessive\ deformation|PGA) = P(Z_\Delta < 0) \tag{41}$$

The fitted fragility function is plotted from the simulation data using maximum likelihood estimation as shown in Fig. 14. Seismic fragility curves are generated for different reservoir levels ranging from 0 to 5m. These fragility curves can be combined and represented in the form of a seismic fragility surface as shown in Fig. 15. However, the purpose of a seismic fragility surface is to utilize the surface plot in conjunction with the flooding analysis and to develop a fragility surface for the multi-hazard scenario. The combined multi-hazard fragility surface is presented in next section.

Table 3
Selected Ground motions

Location	Station
Parkfield, 1966	Cholame - Shandon Array #12
San Fernando, 1971	Lake Hughes #12
Oroville-01, 1975	Oroville Seismograph Station
Friuli Italy-01, 1976	Tolmezzo
Gazli USSR, 1976	Karakyr
Tabas Iran, 1978	Dayhook
Norcia Italy, 1979	Cascia
Nahanni Canada, 1985	Site 2
Nahanni Canada, 1985	Site 3
Baja California, 1987	Cerro Prieto

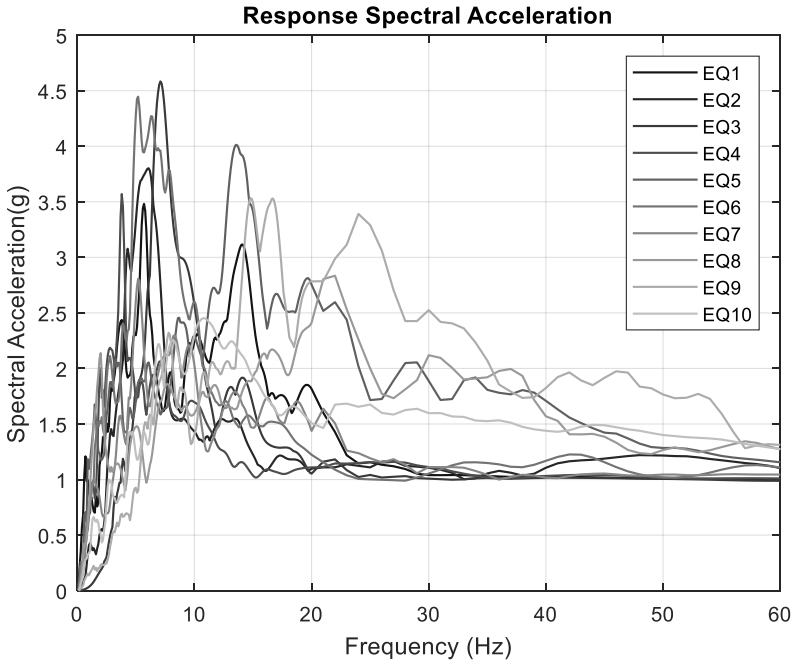

Fig. 13. Response Spectral acceleration of selected Ground motions.

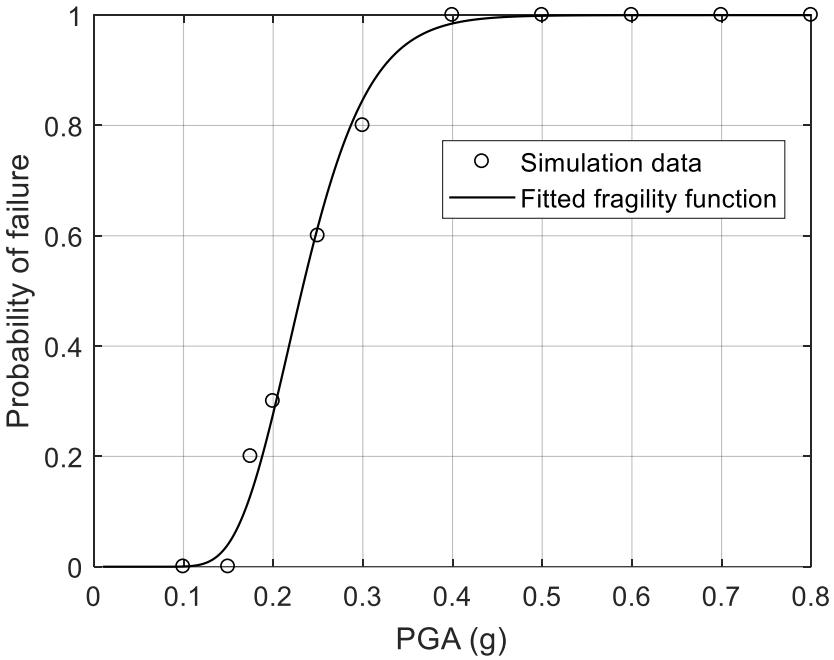

Fig. 14. Fragility curve due to Excessive Deformation failure mode for a flood level of 2.5 m.

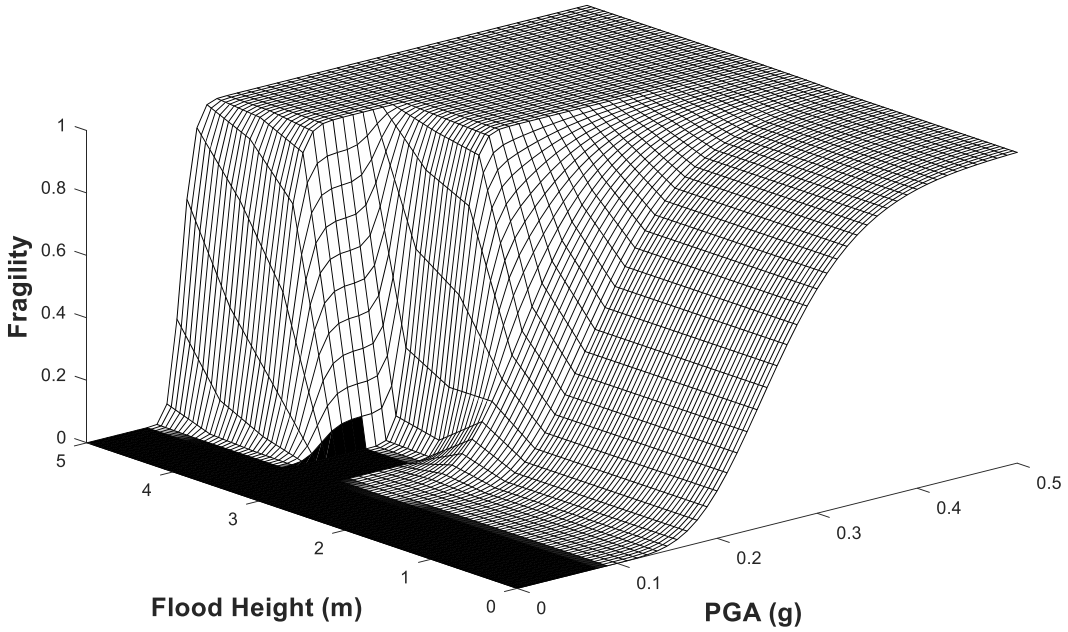

Fig. 15. Seismic Fragility Surface due to Excessive Deformation failure mode.

5. Multi-hazard fragility assessment

A multi-hazard analysis is essential for determining the overall risk of the floodwall against all possible hazards. The probability of failure due to multiple hazards is evaluated by appropriately

combining the probabilities of failure due to each hazard. A multi-hazard fragility surface (Fig. 16) is obtained by combining the seismic fragility surface (Fig. 15) and the system level flooding fragility curve (Fig. 7) using the following expression.

$$P(system) = \bigcup_i P(sytem_i|hazard) \tag{42}$$

where, $P(system_i|hazard)$ is the system fragility of i^{th} hazard.

The floodwall can fail due to flooding hazard even without any seismic load. For lower magnitudes of flood height, the seismic hazard takes over the flooding hazard. However, the floodwall does not fail in seismic until it reaches a certain magnitude of PGA.

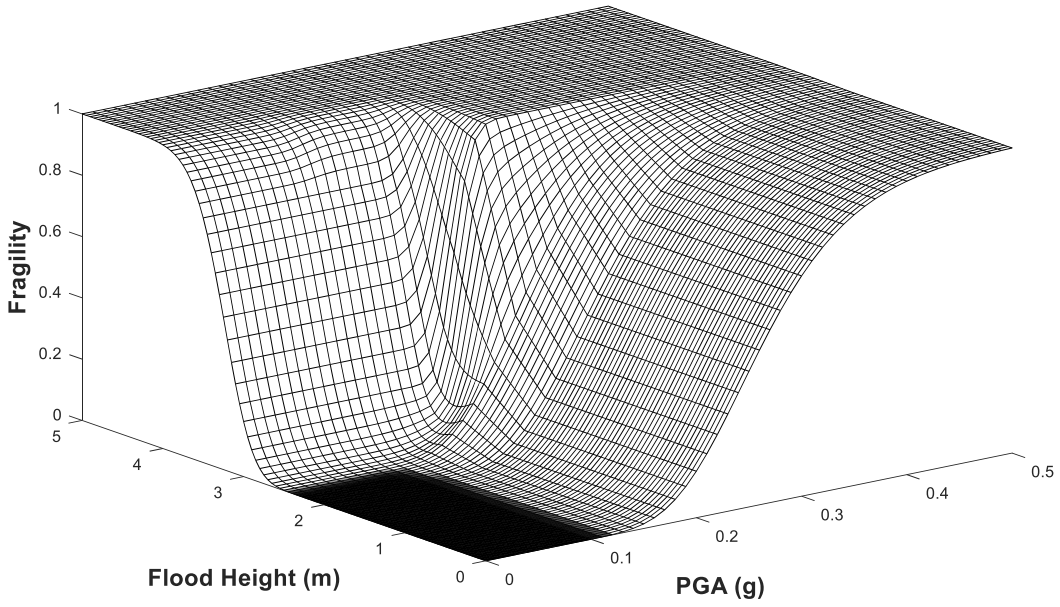

Fig. 16. Multi-hazard Fragility Surface.

6. Conclusions

The conclusions related to the fragility of a concrete floodwall considering various comprehensive set of failure modes under a multi-hazard scenario of flooding and seismic events are:

- There is no failure in overturning of the floodwall and compression failure of concrete at the toe of the floodwall.
- For Class 2 soil, the flooding fragility curves due to sliding of the floodwall and compression failure of foundation at the toe are almost zero for the functional height (around 4 m) of upstream water level.
- For the system level flooding fragility, the relative contribution of rupture failure mode is higher than other failure modes.

- The seismic fragility of a concrete floodwall is highly dependent upon the fluid-structure interaction.
- The seismic fragilities obtained for excessive deformation failure mode of the floodwall fit quite well with the cumulative lognormal distribution. The results indicate a median seismic fragility of 0.23g with a standard deviation of 0.25.
- For different heights of the reservoir level, the seismic fragility curve changes to a fragility surface.
- From the multi-hazard fragility surface, the probability of system failure can be obtained for the corresponding flood height and peak ground acceleration.

References

[1] Tekie PB, Ellingwood BR. Seismic fragility assessment of concrete gravity dams. Earthq Eng Struct Dyn 2003;32:2221–40. https://doi.org/10.1002/eqe.325.

[2] Lupoi A, Callari C. A probabilistic method for the seismic assessment of existing concrete gravity dams. Struct Infrastruct Eng 2011:1–14. https://doi.org/10.1080/15732479.2011.574819.

[3] Ju BS, Jung W. Evaluation of Seismic Fragility of Weir Structures in South Korea. Math Probl Eng 2015;2015:1–10. https://doi.org/10.1155/2015/391569.

[4] Kaida H, Miyagawa Y, Kihara N. Methodology for Fragility Evaluation of a Seawall Against Tsunami Effects: Part 1 — Overflow and Physical Damage Associated With Tsunami Wave Pressure. Vol. 2 Smart Grids, Grid Stability, Offsite Emerg. Power; Adv. Next Gener. React. Fusion Technol. Safety, Secur. Cyber Secur. Codes, Stand. Conform. Assessment, Licens. Regul. Issues, American Society of Mechanical Engineers; 2016. https://doi.org/10.1115/ICONE24-60927.

[5] Rajabalinejad M, Van Gelder P, Vrijling JK. Probabilistic finite elements with dynamic limit bounds; a case study: 17th Street flood wall, New Orleans. Civil, Archit Environ Eng 2008.

[6] FEMA P-259. Engineering Principles and Practices of Retrofitting Flood-Prone Residential Structures. Third Edit. 2012.

[7] Sandhu HK. Flooding Fragility of Concrete Gravity Dam-Foundation System. North Carolina State University, 2015.

[8] ASTM D2487-00. Standard classification of soils for engineering purposes (Unified Soil Classification System). ASTM Int West Conshohocken, PA 2000. https://doi.org/https://doi.org/10.1520/D2487-00.

[9] Terzaghi K. Theoretical Soil Mechanics. Hoboken, NJ, USA: John Wiley & Sons, Inc.; 1943. https://doi.org/10.1002/9780470172766.

[10] Bodda Saran Srikanth. Multi-Hazard Risk Assessment of a Flood Defense Structure. 2017.

[11] Bodda SS, Sandhu HK, Gupta A. Fragility of a Flood Defense Structure Subjected to Multi-Hazard Scenario. Vol. 4 Comput. Fluid Dyn. Coupled Codes; Decontam. Decommissioning, Radiat. Prot. Shield. Waste Manag. Work. Dev. Nucl. Educ. Public Accept. Mitig. Strateg. Beyond, American Society of Mechanical Engineers; 2016. https://doi.org/10.1115/ICONE24-60508.

[12] Akhaveissy AH, Malekshahi M. Transient analysis of dam-reservoir interaction. IACSIT Coimbatore Conf., 2012, p. 183–7.

[13] Khosravi S, Heydari MM. Modelling of concrete gravity dam including dam-water-foundation rock interaction. World Appl Sci J 2013;22:538–46. https://doi.org/10.5829/idosi.wasj.2013.22.04.551.

[14] Fenves G, Chopra AK. Effects of reservoir bottom absorption on earthquake response of concrete gravity dams. Earthq Eng Struct Dyn 1983;11:809–29. https://doi.org/10.1002/eqe.4290110607.

[15] Orlanski I. A simple boundary condition for unbounded hyperbolic flows. J Comput Phys 1976;21:251–69. https://doi.org/10.1016/0021-9991(76)90023-1.

[16] ANSYS (R16.2) Mechanical APDL Theory Reference. n.d.

[17] Zeidan BA. Hydrodynamic analysis of concrete gravity dams subjected to ground motion. 9th Symp. ICOLD Eur. Club. Club IECS201310-12 April. Italy, 2013.

[18] Antunes do Carmo JS, de Carvalho RF. Large dam-reservoir systems: guidelines and tools to estimate loads resulting from natural hazards. Nat Hazards 2011;59:75–106. https://doi.org/10.1007/s11069-011-9740-9.